Journal of Bio- and Tribo-Corrosion (2022) 8:114
https://doi.org/10.1007/s40735-022-00715-8

Formulation of Magnesium Conversion Coating with Herbal Extracts for Biomedical Applications

Saranya Kannan[1] · Kalaiyarasan Madhu[2] · Rajendran Nallaiyan[3]

Received: 11 April 2022 / Revised: 16 September 2022 / Accepted: 12 October 2022 / Published online: 19 October 2022

Abstract
Magnesium and its alloys are one of the most reliable biodegradable implant materials with good mechanical properties. The rapid corrosion behaviour of Mg in the physiological fluid prevents its usage. The corrosion resistance and biocompatibility of the AZ31 Magnesium alloy are enriched with conversion coatings formulated with the extract of *Terminalia chebula*. The surface of AZ31 Mg alloy was treated with sodium hydroxide followed by the treatment with ethanolic extract of *T. chebula*. The coating showed thallus-like morphology. The interaction of Mg with the tannins and phytates present in the extract was confirmed with Attenuated Total Reflectance Infrared spectra. In the coating, the corrosion rate was effectively declined due to the passive layer formed as a result of the chelation of Mg^{2+} ions by the phytate and tannate. The coating exhibited apatite forming ability.

Keywords AZ31 Magnesium alloy · Organic conversion coating · Corrosion analysis · Apatite

1 Introduction

The comprehensive properties of Mg such as similar Young's modulus to that of bone, non-toxicity, etc., make them an unavoidable material in the biomedical field [1–5]. The possible usage of Magnesium as an implant in various fields including cardiovascular, musculoskeletal ligature, vascular stents, orthopaedics and bio-batteries for pacemakers was recommended widely [6]. It does not necessitate revision surgery thereby reducing the duration of physical disability [7, 8]. The high reactivity and rapid corrosion of Mg alloy in the physiological fluid hinder the usage in biomedical field due to the increase in alkalinity on the local sites and hydrogen evolution [9, 10]. To establish better corrosion resistance, surface treatments were widely done.

Conversion coating is a widely used technique to reduce the corrosion rate [11, 12]. The green conversion coating has gained eminence in recent days due to the employment of environment-friendly non-toxic biological macromolecules [13–15]. The organic compounds isolated from the plant source were effective in inhibiting corrosion [16–18]. *Terminalia chebula*, king of medicine, possess various medicinal properties including antibacterial, antioxidant and anticancer activities. The extract of *T. chebula* consists of various bioactive compounds of tannin, phenolic acid and flavonoids [19]. Tannins and phytic acids have effectively reduced the corrosion rate of corrosion in Mg alloy [20]. Tannin/hydroxyapatite coating on AZ31 Mg alloy was prepared by chemical conversion coating to improve the bioactivity and corrosion resistance [21]. The gallic acid and hexamethylene diamine coating on Magnesium alloy were effective in reducing the corrosion rate [22]. The organic acids react with magnesium and form the corresponding magnesium compound, which is merely insoluble and prevents the metal from degradation [23]. The phenolic network on MgZn alloy was efficient in mitigating the hydrogen evolution and was quite stable in *in-vivo* conditions [24]. In the present work, we formulate a conversion coating with the ethanolic extract

✉ Saranya Kannan
saranyak.sdc@saveetha.com

[1] Functional Nanobiomaterials Laboratory (Green Lab), Department of Periodontics, Saveetha Dental College and Hospitals, Saveetha Institute of Medical and Technical Sciences (SIMATS), Saveetha University, Chennai, Tamil Nadu, India

[2] Department of Oral Pathology, Saveetha Dental College and Hospitals, SIMATS, Saveetha University, Chennai, India

[3] Department of Chemistry, CEG Campus, Anna University, Chennai, Tamilnadu, India

of *T. chebula* on AZ31 Mg alloy and the corrosion behaviour and apatite forming ability of the coating were studied.

2 Materials and Methods

2.1 Formation of Gadolinium Conversion Coating

AZ31 Magnesium alloy was obtained from Seoul National University, South Korea. The chemical composition of the AZ31 Mg alloy was Al (2.83%), Zn (0.8%), Mn (0.37%), Cu (0.002%) and remaining Mg. The metal sheets were cut into metal coupons of dimensions 15 mm × 25 mm × 1 mm. The sample surface was mechanically polished with emery sheets (600 to 1200 grits) to remove the oxide layer. Then, the samples were thoroughly washed with acetone using a sonicator. The prepared samples were soaked in 1 N sodium hydroxide solution for 20 min in an upright position to form an oxide layer on the surface.

Terminalia chebula was obtained from the local market. The ethanolic extract of *T. chebula* was prepared by dissolving 5 g of the powder in 100 ml of ethanol (Hayman, Premium grade ethanol 100%) and stirred for about 2 h in room temperature. Then the solution was filtered and the extract was employed for the preparation of the organic conversion coating. The prepared sample was soaked in upright position on the extract solution for 40 min at room temperature to ensure that the entire surface was covered with the extract solution, and then was washed with distilled water and placed in the desiccator.

2.2 Surface and Physicochemical Characterizations

High-Resolution Scanning Electron Microscope with Energy-Dispersive X-ray spectroscopy (SEM/EDX), FEI Quanta FEG 200 was employed to monitor the surface morphology of the coating. The coated sample was sputtered with gold for 20 s before SEM analysis. Fourier Transform Infrared spectrometer with a single reflection ATR accessory (Perkin Elmer Spectrum two, USA) was used to identify the functional groups of the coating. The samples were scanned in the range of 4000–450 cm^{-1} with a spectral resolution of 0.2 cm^{-1}. The crystallographic morphology of the coated sample was analysed with grazing incidence X-ray diffraction (Empyrean, Malvern Panalytical**,** United Kingdom) using CuK radiation.

2.3 Electrochemical Studies

The electrochemical studies were carried out using potentiostat/galvanostat (PGSTAT model 302 N, AUTOLAB, Netherlands) connected to a personal computer with Nova 2.0 software. The three-electrode system was employed in which the sample acts as the anode, platinum as the cathode and saturated calomel electrode as the reference electrode. The preparation of simulated body fluid (SBF) was discussed in our previous literature [4] and employed as the electrolyte. The samples were placed in a specially designed corrosion cell in which the exposed surface area was 1 cm^2 to perform all the electrochemical studies. The open-circuit potential of the samples was monitored for a period of 30 min by immersing in SBF. The electrochemical impedance spectroscopic studies were executed in the frequency range of 100 kHz–10 mHz with an amplitude of the sinusoidal wave of 10 mV on OCP. The obtained electrical impedance data were fitted with ZSimpwin 3.21 version software to acquire the parameters that provide the information on the interphase/electrode environment. Potentiodynamic polarization studies were done with a scan rate of 1 mV/s from 500 mV of OCP till the breakdown of the coating. The slopes of the curves (β_a and β_c) were obtained by drawing slopes with the aid of NOVA 2.0 software. The polarization resistance was determined by using the Stern–Geary equation [25].

$$R_p = \frac{\beta_a \times \beta_c}{2.3 i_{corr}\left(\beta_a + \beta_c\right)}, \tag{1}$$

where β_a and β_c are slopes of anodic and cathodic parts of the polarization plots in V/dec; R_p is polarization resistance in kΩ.

2.4 Immersion Studies

The organic conversion-coated sample was immersed in the SBF solution for 7 days at 37 °C. The SBF solution was changed on alternate days. HR-SEM/EDX and ATR-IR were performed to ensure apatite formation on the surface.

3 Results and Discussions

3.1 Topographical Analysis

Figure 1 shows the SEM image of herbal extract conversion coating on Mg alloy. The coating displayed the thallus-like morphology. The cracks are seen on the surface due to dehydration and surface shrinkage. The cross section of the organic conversion coating showed that the thickness of the coating was ~ 14.5 µm. The elemental analysis shows the uniform distribution of carbon, nitrogen, oxygen and magnesium.

The functional groups of the ethanolic extract of *T.chebula* and conversion coating formed on AZ31 Mg alloy are given in Fig. 2. The ethanol extract of *T. chebula* showed

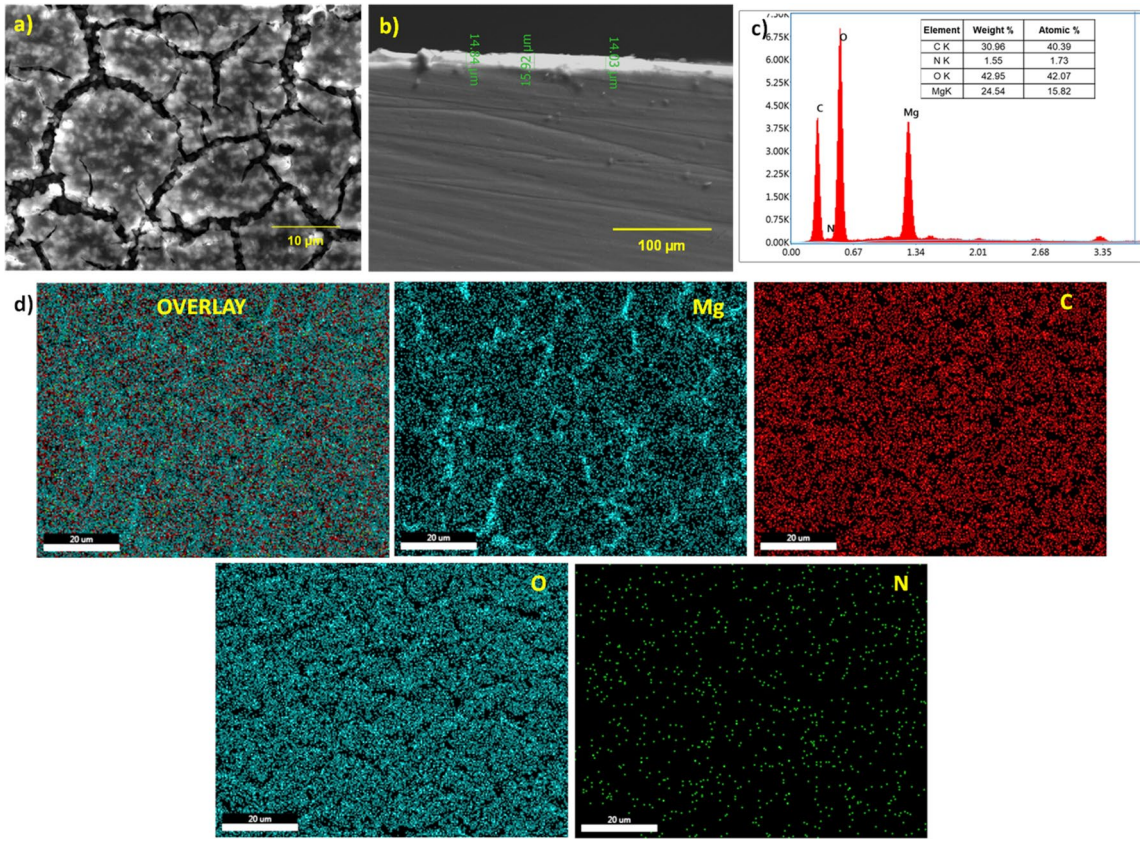

Fig. 1 SEM images (**a**), cross section (**b**), EDX profile (**c**) and mapping (**d**) of organic conversion coating

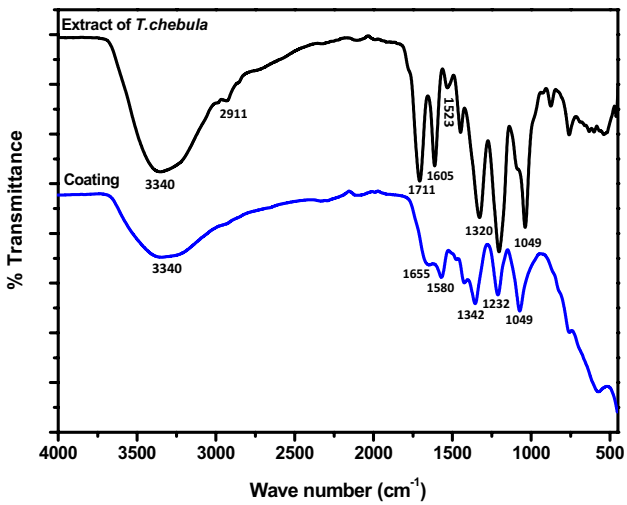

Fig. 2 The chemical interaction on the organic conversion coating formation determined using ATR-IR spectra of *T. chebula* extract and organic conversion coating

a broad peak at 3340 cm^{-1} corresponding to the hydroxyl group (–OH) [27]. The saturated –CH stretching of the polyol is seen at 2911 cm^{-1} [28]. The phenolic compounds are observed at 1320, 1232 and 1174 cm^{-1}. The characteristic peaks of amines are seen at 1605 and 1523 cm^{-1}. The peaks at 1711 cm^{-1} signify the presence of the carboxylic acid (–C = O) group and the glycosidic linkages are at 1049 cm^{-1} [29]. The significant peak shift from 1523 to 1580 cm^{-1} and 1605 to 1655 cm^{-1} indicates the coating formed on the surface [30]. The tannins are weak acids that effectively react with the metal and form a coating on the surface. The tannins present in the extract of *T. chebula* have the ability to chelate with Mg^{+} ions by bonding with –OH groups of the aromatic rings; thereby developing a highly cross-linked passive layer of hydroxybenzoic acid magnesium [26]31.

The X-ray diffraction (XRD) analysis of the conversion coating on Mg alloy is shown in Fig. 3. The International centre for diffraction data (ICDD) card no. 01-079-6692 matches with the base metal magnesium. The crystal cubic structure of MgO showed peaks at 36.9° and 78.3°, which matches with the ICDD card no. 045-0946 [32]. The broad peak around 20° indicates the formation of coating in the amorphous state.

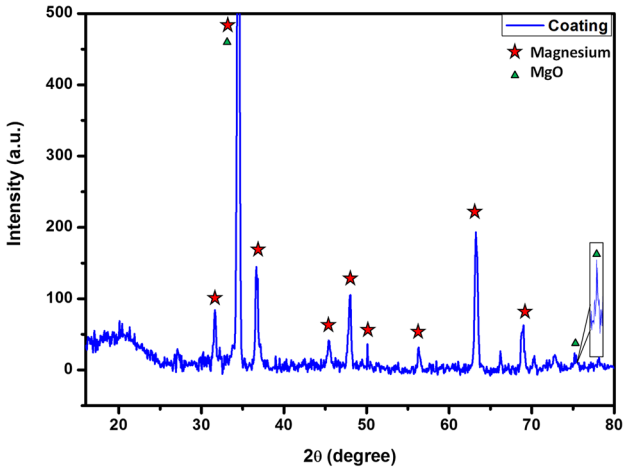

Fig. 3 The crystallographic pattern of the organic conversion coating

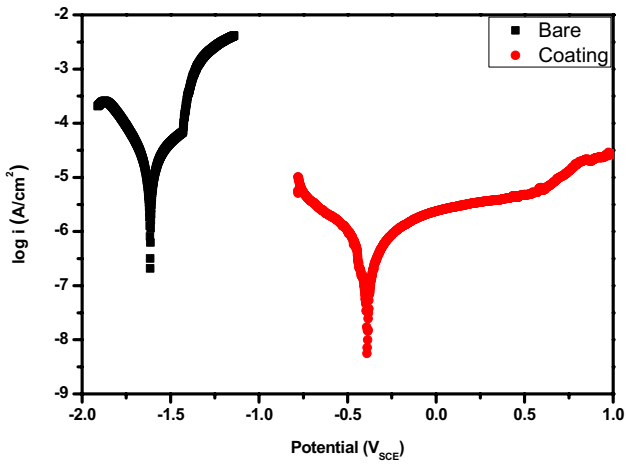

Fig. 4 Potentiodynamic polarization curve of the bare and organic conversion coating in SBF solution

3.2 Electrochemical Studies

Figure 4 provides potentiodynamic polarization plot of the bare and coated sample and the corresponding data are provided in Table 1. The coated sample was compared with the bare reported in our previous work [33]. The potentiodynamic polarization curve was analysed with NOVA 2.0 software and the corrosion current (i_{corr}), corrosion potential (E_{corr}), polarization resistance (R_p) and corrosion rate (C_R). The corrosion rate of the coating (0.012 mm/yr) has considerably declined in comparison to the bare (0.962 mm/yr). The anodic current density was lower than the cathodic current density for both coated and bare. A positive shift in the corrosion potential was observed in the coated sample than bare. The oxide layer on the surface of Mg alloy breaks down at the potential of − 1.42 V, whereas the coating breaks down at 0.59 V. The coating can withstand a large potential range indicating that they have the ability to withstand the dynamic potential generated during the bone remodelling [34–36]. The protection efficiency was calculated and found to be 98.75%. The results indicate that the penetration of the physiological fluids was hindered by the passive layer formed on the surface [37].

Figure 5 shows the Nyquist and Bode plots obtained from EIS studies. There is a correlation between the capacitance loop in the high-frequency region and corrosion rate. The capacitive semicircle diameter is proportional to the corrosion resistance of the material. The semicircle diameter in the high-frequency region of the coating was bigger than the bare indicating that the corrosion rate was slowed down by the passive coating layer.

The obtained EIS spectra were matched with electrochemical equivalent circuits (EEC) fitted with the electrochemical equivalent circuits with the chi-square value of 10^{-4} to 10^{-3} and the acquired data are given in Table 2. R_s illustrates the solution resistance; In bare, R_1, R_2 and R_L signify the resistance of the natural oxide layer, substrate and inductor resistance. The CPE_1 and CPE_2 are the constant phase angle element of the natural oxide layer and substrate, respectively. L represents the inductance on the substrate. In coating, R_1 and R_2 is the resistance offered by the passive coating layer and the substrate. The corresponding constant phase angle elements are represented as CPE_1 and CPE_2.

By combining Nyquist and Bode plots, the bare exhibited two capacitive loops and an inductive loop. The first capacitive semicircle of the bare was formed as a result of charge transfer in the partially formed oxide/hydroxide layer on the substrate and electrolyte, while the second capacitive loop was attributed to the mass transport relaxation of the oxide/hydroxide layer. The inductive loop was obtained as a result of adsorption/desorption of Mg^+ species on the surface which initiates pitting corrosion [38]. The first capacitive loop of the coating

Table 1 Potentiodynamic polarization data of bare and organic conversion coating sample

S.No	Sample	E_{corr} (V)	i_{corr} (μA/cm^2)	Corrosion rate, C_R (mm/yr)	Polarization resistance, R_p (KΩ)	Breakdown, B_d (V)	Protection efficiency (%)
1.	BARE	− 1.611	42.5	0.962	2.141	− 1.42	–
2.	COATING	− 0.389	0.53	0.012	184.013	0.59	98.75

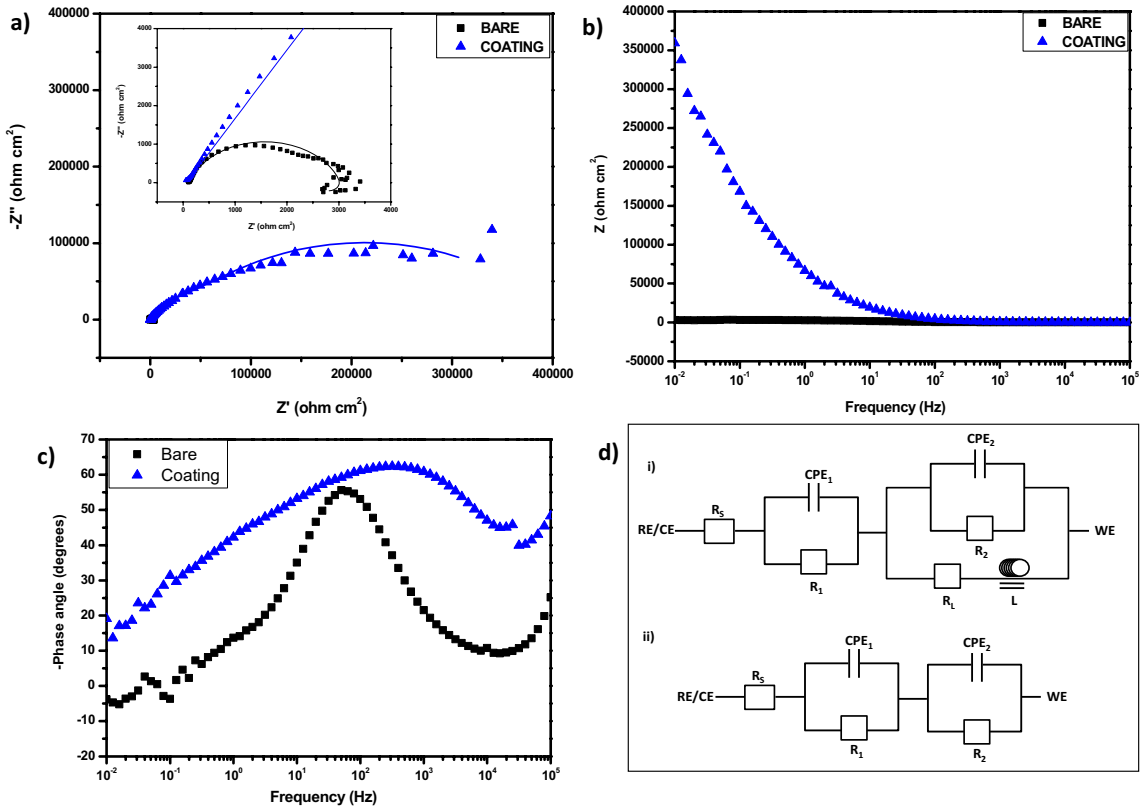

Fig. 5 Corrosion behaviour of the organic conversion coating was determined from Nyquist (**a**), Bode impedance (**b**) and phase angle (**c**). The corresponding equivalent circuit (**d**) of bare and coating

Table 2 Electrochemical impedance data of bare and coating obtained by fitting with the equivalent electrochemical circuits

Sample	CPE_1 (μS s^n cm^{-2})	n_1	R_1 (kΩ cm^2)	CPE_2 (μS s^n cm^{-2})	n_2	R_2(kΩ cm^2)	L (H)	R_L(kΩ cm^2)
Bare	5.02	0.848	0.112	16.12	0.799	2.476	7189	0.449
Coating	3.49	0.616	24.65	6.30	0.852	380.8	–	–

in the high-frequency region reflects the electrical double layer and the second capacitive loop in the mid- and low-frequency region signifying the resistive behaviour of the coating. The bare showed a resistance value of 2.588 KΩ indicating their poor resistance in the SBF solution, whereas the coating showed a higher resistance of 405.5 KΩ. The chelation of Mg^{2+} ions by the organic compounds on the conversion coating impedes the ionic movement from the coating and also from the solution by forming a barrier [30].

In the Bode phase angle plot, the bare showed an initial phase angle of 23° in the high-frequency region and reaches a maximum of 54° in the mid-frequency region and drops down to − 4° in the low-frequency region. The negative phase angle in the low frequency signifies the rapid dissolution of Mg from the bare. In the coating, the phase angle begins at 46° and attains 67° in the mid-frequency; then reaches 19° in the low-frequency region. The disappearance of the inductive loop was seen on the coating. The phytate and tannate complex on the coating surface prevents the release of Mg^{2+} ions from the substrate through the electrostatic interactions [26, 39]. Therefore, the corrosion behaviour of the material was improved.

3.3 Apatite Forming Ability

The organic conversion coating was immersed in SBF for 7 days. The surface morphology analysed using SEM/EDX and the functional group by ATR-IR analysis are given in Fig. 6. The clustered aggregates of nanospherical apatite

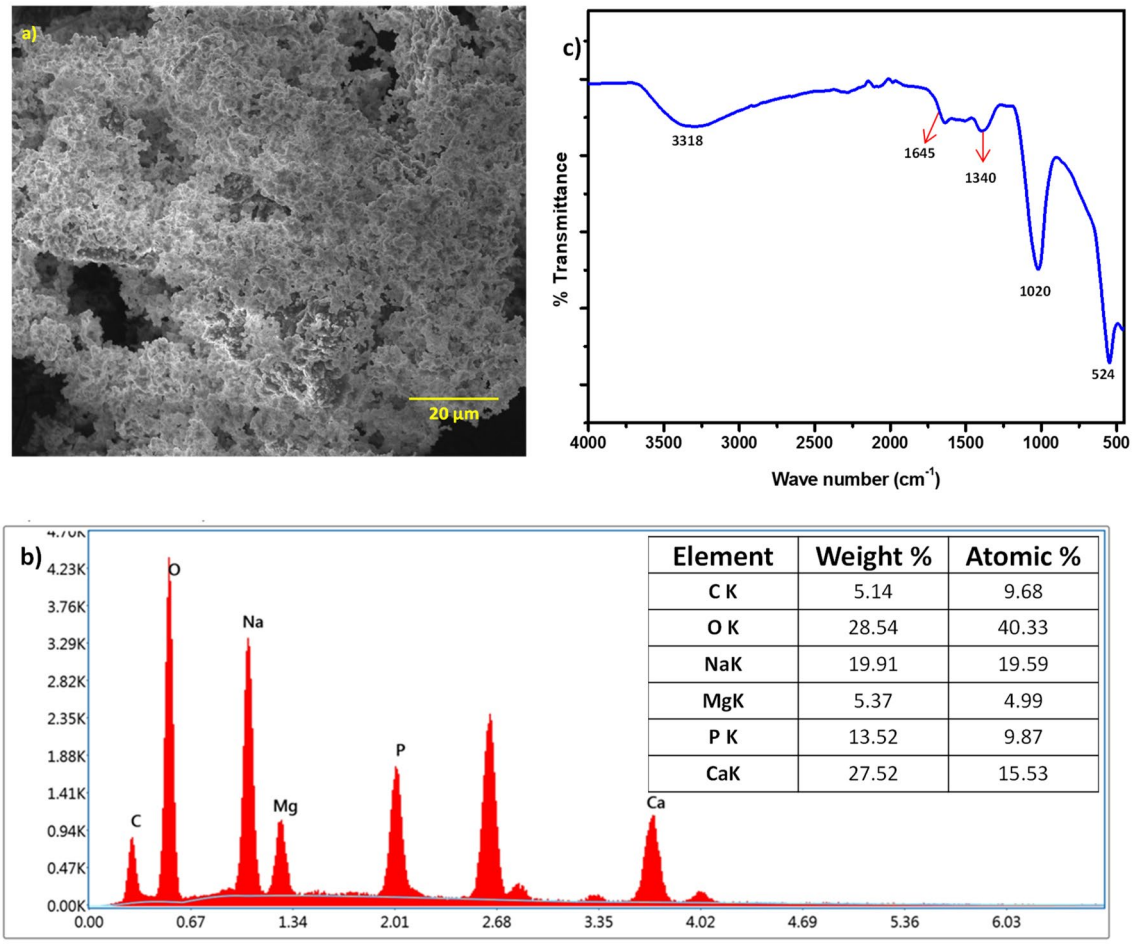

Element	Weight %	Atomic %
C K	5.14	9.68
O K	28.54	40.33
NaK	19.91	19.59
MgK	5.37	4.99
P K	13.52	9.87
CaK	27.52	15.53

Fig. 6 Apatite formation on the organic conversion coating after immersion in SBF for 7 days—SEM image (**a**), EDX profile (**b**) and ATR-IR spectrum (**c**)

deposition are seen on the surface (given as in Fig. 6a, b). The existence of carbon, oxygen, sodium, calcium, phosphorous and magnesium was identified indicating the apatite forming the ability of the organic conversion coating.

The possible apatite formation mechanisms are (i) the glycosidic linkages on the conversion coating of the Mg surface indicate the adsorption of sugar molecules during the coating formation. When the coating is placed in SBF, the glucose converts into gluconic acid, which in turn recruits the Ca^{2+} ions [15]. (ii) The conversion coating formed on the surface consists of polyphenolic compounds including tannates and phytates, which chelate with the Ca^{2+} ions. The recruited Ca^{2+} binds with the negatively charged phosphate ions in a co-ordinate fashion leading to the deposition of apatite [40]. From the ATR-IR spectrum (Fig. 6c), the 7-day immersion sample of the coating exhibited the peaks at 3318, 1645 and 1340 attributed to hydroxyl group, amines and phenolic compounds. The two new peaks apart from the organic coating peaks at 1020 and 524 cm^{-1} correspond to the γ3 and γ4 vibrations of the phosphate [41]. Hence, it is confirmed that the coating has the ability to support the apatite formation.

4 Conclusion

The organic conversion coating was formulated with the extract of *T. chebula* on AZ31 Mg alloy. The following observations and conclusions were derived from the work.

- The conversion coating formed the thallus-like morphology. The coating surface showed the presence of amines, phenols, carboxylic and hydroxyl groups along with glycosidic linkages confirming the formation of the conversion coating in the amorphous state.
- The coating was effective in enhancing the corrosion resistance in 'limited' in-vitro conditions. Also, the coating has the ability to support the apatite formation on the surface by chelating the ions from the SBF solution.

Overall, the coating with the herbal extract can be a simple and effective method that can be employed in bio-implants.

Acknowledgements The Instrumentation facilities provided by DST-FIST and UGC-DRS to Department of Chemistry, Anna University, Chennai, India are gratefully acknowledged.

Author Contribution KS: Conceptualization, Methodology and Writing—original draft; MK: Methodology and Writing—review & editing; NR: Investigation and Supervision.

Funding This research received no specific grant from any funding agency in the public, commercial or not-for-profit sectors.

Data Availability The datasets generated during and/or analysed during the current study are available from the corresponding author on reasonable request.

Declarations

Competing interest The authors declare that they have no known competing financial interests or personal relationships that could have appeared to influence the work reported in this paper.

References

1. Babaremu K, John M, Mfoh U, Akinlabi E, Okokpujie I (2021) Behavioral characteristics of magnesium as a biomaterial for surface engineering application. J Bio- Tribo-Corros 7:1–12
2. Mahapatro A, Arshanapalli SA (2017) Bioceramic coatings on magnesium alloys. J Bio- Tribo-Corros 3:1–9
3. Kalaiyarasan M, Saranya K, Rajendran N (2020) In-vitro corrosion assessment of silicate-coated AZ31 Mg alloy in Earle's solution. J Mater Sci 55:3571–3587
4. Saranya K, Bhuvaneswari S, Chatterjee S, Rajendran N (2021) Titanate incorporated anodized coating on magnesium alloy for corrosion protection, antibacterial responses and osteogenic enhancement. J Magnes Alloys 10:1109
5. Liang C, Zheng R, Huang N, Xu L (2009) Conversion coating treatment for AZ31 magnesium alloys by a phytic acid bath. J Appl Electrochem 39:1857–1862
6. Sudha M, Surendhiran S, Gowthambabu V, Balamurugan A, Anandarasu R, Syed Khadar Y, Vasudevan D (2021) Enhancement of corrosive-resistant behavior of Zn and Mg metal plates using biosynthesized nickel oxide nanoparticles. J Bio- Tribo-Corros 7:1–16
7. Li Q, Bao X, Je S, Cai S, Xie Y, Liu Y, Liu J, Xu G (2021) Fabrication of superhydrophobic composite coating of hydroxyapatite/stearic acid on magnesium alloy and its corrosion resistance, antibacterial adhesion. J Mater Sci 56:5233–5249
8. Kannan S, Nallaiyan R (2020) Anticancer activity of Samarium-coated magnesium implants for immunocompromised patients. ACS Appl Bio Mater 3:4408–4416
9. Saranya K, Kalaiyarasan M, Rajendran N (2019) Selenium conversion coating on AZ31 Mg alloy: a solution for improved corrosion rate and enhanced bio-adaptability. Surf Coat Technol 378:124902
10. Zhang X, Zhao Z, Wu F, Wang Y, Wu J (2007) Corrosion and wear resistance of AZ91D magnesium alloy with and without microarc oxidation coating in Hank's solution. J Mater Sci 42:8523–8528
11. Qian Z, Wang S, Wu Z (2017) Corrosion behavior study of AZ31B magnesium alloy by sol-gel silica-based hybrid coating. Int J Electrochem Sci 12:8269–8279
12. Francis A, Yang Y, Boccaccini A (2019) A new strategy for developing chitosan conversion coating on magnesium substrates for orthopedic implants. Appl Surf Sci 466:854–862
13. Lu Y, Feng H, Xu H (2021) Studying corrosion and adhesion performance of a phytic acid based conversion coating post-treated with garlic extract on Q235 steel. Int J Electrochem Sci. https://doi.org/10.20964/2021.04.43
14. Ghoreishiamiri S, Raja PB, Ismail M, Hashemi Karouei SF (2020) Properties of contaminated reinforced concrete added by areca catechu leaf extract as an eco-friendly corrosion inhibitor. J Bio-Tribo-Corros 6:1–14
15. de Sampaio MT, Fernandes CM, de Souza GG, Carvalho ES, Velasco JA, Silva JCM, Alves OC, Ponzio EA (2021) Evaluation of aqueous extract of Mandevilla fragrans leaves as environmental-friendly corrosion inhibitor for mild steel in acid medium. J Bio- Tribo-Corros 7:1–11
16. Jessima S, Subhashini S, Arulraj J (2020) Sunova spirulina powder as an effective environmentally friendly corrosion inhibitor for mild steel in acid medium. J Bio- Tribo-Corros 6:1–13
17. Ayoola A, Fayomi O, Akande I, Ayeni O, Agboola O, Obanla O, Abatan O, Chukwuka C (2020) Inhibitive corrosion performance of the eco-friendly aloe vera in acidic media of mild and stainless steels. J Bio- Tribo-Corros 6:1–13
18. Ojha LK, Tüzün B, Bhawsar J (2020) Experimental and theoretical study of effect of Allium sativum extracts as corrosion inhibitor on mild steel in 1 M HCl medium. J Bio- Tribo-Corros 6:1–10
19. Nigam M, Mishra AP, Adhikari-Devkota A, Dirar AI, Hassan MM, Adhikari A, Belwal T, Devkota HP (2020) Fruits of *Terminalia chebula* Retz.: a review on traditional uses, bioactive chemical constituents and pharmacological activities. Phytother Res 34:2518–2533
20. Saji VS (2019) Organic conversion coatings for magnesium and its alloys. J Ind Eng Chem 75:20–37
21. Zhu B, Wang S, Wang L, Yang Y, Liang J, Cao B (2017) Preparation of hydroxyapatite/tannic acid coating to enhance the corrosion resistance and cytocompatibility of AZ31 magnesium alloys. Coatings 7:105
22. Chen S, Zhao S, Chen M, Zhang X, Zhang J, Li X, Zhang H, Shen X, Wang J, Huang N (2019) The anticorrosion mechanism of phenolic conversion coating applied on magnesium implants. Appl Surf Sci 463:953–967
23. Abatti GP, Pires ATN, Spinelli A, Scharnagl N, da Conceição TF (2018) Conversion coating on magnesium alloy sheet (AZ31) by vanillic acid treatment: preparation, characterization and corrosion behaviour. J Alloy Compd 738:224–232
24. Asgari M, Yang Y, Yang S, Yu Z, Yarlagadda PK, Xiao Y, Li Z (2019) Mg–phenolic network strategy for enhancing corrosion resistance and osteocompatibility of degradable magnesium alloys. ACS Omega 4:21931–21944
25. Abdel-Gawad SA, Shoeib MA (2019) Corrosion studies and microstructure of Mg− Zn− Ca alloys for biomedical applications. Surfaces and Interfaces 14:108–116
26. Mabrour J, Akssira M, Azzi M, Zertoubi M, Saib N, Messaoudi A, Albizane A, Tahiri S (2004) Effect of vegetal tannin on anodic copper dissolution in chloride solutions. Corros Sci 46:1833–1847
27. Nassar A, Hassan A, Shoeib M (2015) Synthesis, characterization and anticorrosion studies of new homobimetallic Co (II), Ni (II), Cu (II), and Zn (II) Schiff base complexes. J Bio- Tribo-Corros 1:1–16
28. Lee H-S, Jung S-H, Yun B-S, Lee K-W (2007) Isolation of chebulic acid from *Terminalia chebula* Retz. and its antioxidant effect in isolated rat hepatocytes. Arch Toxicol 81:211–218

29. Krithiga G, Hemalatha T, Deepachitra R, Ghosh K, Sastry T (2014) Study on osteopotential activity of *Terminalia arjuna* bark extract incorporated bone substitute. Bull Mater Sci 37:1331–1338
30. Chen S, Zhang J, Chen Y, Zhao S, Chen M, Li X, Maitz MF, Wang J, Huang N (2015) Application of phenol/amine copolymerized film modified magnesium alloys: anticorrosion and surface biofunctionalization. ACS Appl Mater Interfaces 7:24510–24522
31. Zhang S, Zhang R, Li W, Li M, Yang G (2012) Effects of tannic acid on properties of anodic coatings obtained by micro arc oxidation on AZ91 magnesium alloy. Surf Coat Technol 207:170–176
32. Saranya K, Bhuvaneswari S, Chatterjee S, Rajendran N (2020) Biocompatible gadolinium-coated magnesium alloy for biomedical applications. J Mater Sci 55:11582–11596
33. Saranya K, Kalaiyarasan M, Chatterjee S, Rajendran N (2019) Dynamic electrochemical impedance study of fluoride conversion coating on AZ31 magnesium alloy to improve bio-adaptability for orthopedic application. Mater Corros 70:698–710
34. Walsh W, Guzelsu N (1993) Ion concentration effects on bone streaming potentials and zeta potentials. Biomaterials 14:331–336
35. Bassett CAL, Becker RO (1962) Generation of electric potentials by bone in response to mechanical stress. Science 137:1063–1064
36. Pienkowski D, Pollack S (1983) The origin of stress-generated potentials in fluid-saturated bone. J Orthop Res 1:30–41
37. Jomy J, Prabhu D, Prabhu P (2022) Inhibitors incorporated into water-based epoxy coatings on metals for corrosion protection: a review. J Bio- Tribo-Corros 8:1–15
38. Su Y, Lu Y, Su Y, Hu J, Lian J, Li G (2015) Enhancing the corrosion resistance and surface bioactivity of a calcium-phosphate coating on a biodegradable AZ60 magnesium alloy via a simple fluorine post-treatment method. RSC Adv 5:56001–56010
39. Chen X, Li G, Lian J, Jiang Q (2009) Study of the formation and growth of tannic acid based conversion coating on AZ91D magnesium alloy. Surf Coat Technol 204:736–747
40. Zeng RC, Li XT, Li SQ, Zhang F, Han E-H (2015) In vitro degradation of pure Mg in response to glucose. Sci Rep. https://doi.org/10.1038/srep13026
41. Saranya K, Kalaiyarasan M, Agilan P, Rajendran N (2022) Biofunctionalization of Mg implants with Gadolinium coating for bone regeneration. Surf Interf. https://doi.org/10.1016/j.surfin.2022.101948